Anionic surfactant solutions under shear using dissipative particle dynamics

Rachel Hendrikse,[1,2,a] Andrew Bayly,[1] and Peter Jimack[3,2]
[1] *School of Chemical and Process Engineering, University of Leeds, Leeds, LS2 9JT, United Kingdom*
[2] *EPSRC Centre for Doctoral Training in Fluid Dynamics at Leeds, University of Leeds, Leeds, LS2 9JT, United Kingdom*
[3] *School of Computing, University of Leeds, Leeds, LS2 9JT, United Kingdom*

(Dated: 18 May 2023)

We present a dissipative particle dynamics study of surfactant solutions under shear, which allows us to investigate their rheological properties. We consider a variety of concentrations and phase structures, including micellar solutions and liquid crystal phases. It is shown that the viscosity of micellar solutions increases as a function of concentration, in agreement with what is expected from experimental data. We also show that micelles can exhibit shear-thinning behaviour when a shear force is applied, which is a result of micelles breaking down into smaller aggregates. Lamellar and hexagonal phases are found to orientate under the application of shear, in agreement with experimental observations. It is normally suggested that lamellar phases under shear can exhibit a transition between orientations, as the shear rate is increased, usually suggested to be a result of lower viscosity. We calculate the viscosity for different lamellar phase orientations, showing that, although the viscosity of perpendicular orientations is lower than that of parallel orientations, we do not observe a transition to the perpendicular phase at high shear rates. Finally, we show that the choice of Schmidt number has a significant impact on the results, which is of importance for determining the correct behaviour via simulations.

I. INTRODUCTION

Surfactants are common components of a wide range of products, particularly in the cleaning and personal care industries. Above the critical micelle concentration, surfactants self-assemble into different structures (or 'phases') depending on their concentration in aqueous solution. Typical phases include micellar, hexagonal, bi-continuous cubic, and lamellar structures. These different phases have different properties, in particular, the rheological properties of micellar solutions are distinctly different to those of the liquid crystalline mesophases. Since the manufacturing processes for product-containing surfactants most commonly involves the application of shear, understanding the properties of surfactant solutions under shear is of fundamental importance.

In this work, we focus on anionic, sodium lauryl ether sulfate (SLES) surfactants of the form $CH_3(CH_2)_{12}(OCH_2CH_2)_nOSO_3Na$, which are common components of personal care products. The degree of ethoxylation n can vary in commercial products, typically taking a distribution of values. At room temperature, aqueous SLES solutions tend to progress through phase transitions micellar→hexagonal→lamellar[1] with increasing concentration. Cubic phases can appear between the hexagonal and lamellar phases when the degree of ethoxylation is large ($n \geq 3$)[2].

In this work, we present simulations of SLES surfactant solutions under the influence of a shear force. These simulations are performed using dissipative particle dynamics (DPD), a mesoscopic technique which uses soft interaction potentials between coarse-grained molecules to reproduce liquid behaviour. We choose DPD over other simulation techniques, such as molecular dynamics, since DPD is able to reach longer time and length scales than such alternative approaches. This makes DPD ideal for studying the behaviour of surfactants while under shearing.

Experimentally, micellar sodium dodecyl sulfate (SLES with $n = 0$) aqueous solutions are generally reported to be Newtonian, with the viscosity increasing with concentration[3,4]. However, the shear rates in experimental measurements using rotational rheometers are typically significantly lower[5,6] ($\approx 10^{-3} - 10^{3}$ s^{-1}) than those used in simulations[5–7] ($\approx 10^{8} - 10^{12}$ s^{-1}). The shear rates used in the manufacturing process of products containing surfactants are also typically larger than those which can be accessed by standard rheometer measurements. SLES-based products, such as shampoos, are often created using high shear mixers, which can generate shear rates ranging from $10^4 - 10^5$ s^{-1} during the mixing process[8]. For micellar systems the viscosity is expected to be influenced by micellar shape, the concentration of micelles and micellar interactions[3,4,9,10]. Therefore it is of interest whether the application of shear at large shear rates causes any changes to these properties, thereby altering the viscosity of the system. Lyotropic liquid crystalline mesophases typically exhibit very different rheological behaviour, possessing a viscosity which is many orders of magnitude larger than that of micellar systems. They can also show shear-thinning and time-dependent[3,11–16] properties.

A number of existing studies have used DPD to investigate the rheological behaviour of surfactant systems[17–21],

[a] Current address Department of Chemistry, Durham University, Durham, DH1 3LE, United Kingdom.; Electronic mail: rachel.hendrikse@durham.ac.uk

although typically viscosity calculations can only be performed at relatively high shear rates[17,19,21,22], since the viscosity calculation displays a large amount of noise at decreasing shear rates[17,22]. Existing DPD studies predict shear-thinning behaviour for micellar systems[17,18,21], where micelles have been observed to change shape due to the application of a shear force. Spherical micelles can also stretch under shear flow[20], where worm-like micelles can then be broken up into small, spherical micelles at high shear rates, resulting in a lower solution viscosity[17,18]. Using DPD, it has been shown that surfactant molecules can stretch in length as a result of shear[20], meaning that the radius of gyration can be dependent on the shear rate[23]. While existing studies could be found for micellar solutions, there are relatively few prior DPD investigations studying the effect of shear on liquid crystals. Therefore we aim to study solutions across a range of concentrations, specifically the micellar, hexagonal and lamellar phases.

One of the topics of interest in this work is the impact of the Schmidt number, where the Schmidt number Sc is defined as the ratio of kinematic viscosity ν and mass diffusivity D: $\mathrm{Sc} \equiv \nu/D = \mu/\rho D$, where μ is the dynamic viscosity, and ρ is the density. DPD typically generates a Schmidt number which is more comparable to that of a typical gas than a liquid. There is no general consensus in existing literature about how important the Schmidt number is in DPD simulations and the impact it has on results, although it is a topic of interest[24]. In DPD studies of polymer chains[25], it was found that the Schmidt number has no impact on the radius of gyration of molecules R_g when no shear is applied. However, when shear is applied there is a large difference in R_g at different Schmidt numbers. In contrast, other studies have reported that the Schmidt number is unimportant in determining rheology[26], making this a key area of interest.

Experimentally, it is generally reported that the lamellar and hexagonal phases orientate under the application of shear[27–34]. Therefore one of the aims of this work is to investigate the orientation that mesophases take under shear. Lamellar phases have been shown to tend to take one of two orientations, with bilayers stacking either parallel or perpendicular to the direction of flow. For SLE_3S solutions, textures viewed under a polarised optical microscope indicate a parallel alignment under shear[2], which is generally the case for most surfactant systems. Both experiments[31,32,35] and simulation[34] have suggested that, for some systems, there is a transition from the parallel orientation to the perpendicular orientation at very high shear rates (although for other systems the parallel orientation persists at high shear rates[33]). A commonly cited reason for this transition is that the perpendicular orientation[34,35] possesses a lower viscosity. Similarly, hexagonal solutions tend to exhibit two different orientations under shear: either an in-shear-plane orientation or an out-of-shear-plane 'log-rolling' orientation[27]. However, the alignment of hexagonal rods along the flow direction is the most commonly reported preference[28–30].

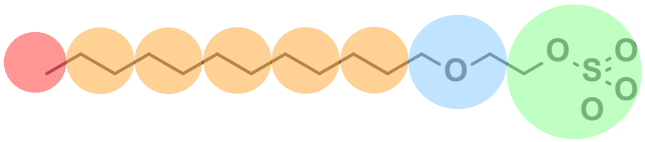

FIG. 1: Coarse-grained representation of SLES molecules used in this work, where beads are coloured according to their type. The number of ethylene oxide beads n is varied.

This article begins with an overview of the DPD method used to simulate SLES solutions at various concentrations. We then provide details on how the viscosity is determined using two approaches: a non-equilibrium method in which shear flow is induced using Lees-Edwards boundary conditions; and an equilibrium method based on pressure fluctuations. We study the impact that shear has on micellar solutions, and how this influences the resulting viscosity. In this study, we vary parameters such as concentration, degree of ethoxylation, shear rate, and Schmidt number. The Schmidt number can be varied with the application of an external thermostat, which can be used to reproduce a Schmidt number closer to that of a realistic fluid than traditional DPD would allow. Finally, we present a study of the impact that applying shear force has on lamellar and hexagonal liquid crystal phases.

II. SIMULATION METHODOLOGY

A. Dissipative particle dynamics

1. Overview

The simulation method of dissipative particle dynamics (DPD) coarse grains molecules, representing groups of atoms as 'beads'. The coarse-graining used in this work for SLES molecules is taken from the parameterisation of Anderson *et al.* (2018)[36], where the coarse-graining is shown in Fig. 1 and water beads represent two water molecules. The head group bead $[CH_2OSO_3^{-1}]^-$ is negatively charged, and the positively charged counter ions Na^+ are partially hydrated with two water beads. The ethylene oxide groups are represented as a single bead $[CH_2OCH_2]$. The alkyl chain is coarse-grained such that one bead represents two carbon atoms $[CH_2CH_2]$ and the alkyl chain is terminated by a bead representing a methyl group $[CH_3]$.

The force on an individual bead from non-bonded interactions is made up of a combination of forces,

$$\mathbf{f}_i = \sum_{j \neq i} (\mathbf{F}_{ij}^{\mathrm{C}} + \mathbf{F}_{ij}^{\mathrm{D}} + \mathbf{F}_{ij}^{\mathrm{R}} + \mathbf{F}_{ij}^{\mathrm{E}}) \tag{1}$$

where $\mathbf{F}_{ij}$ are the forces acting on bead i by bead j. $\mathbf{F}_{ij}^{\mathrm{C}}$ is the conservative force, $\mathbf{F}_{ij}^{\mathrm{D}}$ the dissipative force, $\mathbf{F}_{ij}^{\mathrm{R}}$

the random force, and $\mathbf{F}_{ij}^{\mathrm{E}}$ is the electrostatic force. The conservative force is repulsive and takes the form

$$\mathbf{F}_{ij}^{\mathrm{C}} = \begin{cases} a_{ij}(1 - \frac{r_{ij}}{r_{\mathrm{C}}})\hat{\mathbf{r}}_{ij} & \text{for } r_{ij} < r_{\mathrm{C}} \\ 0 & \text{for } r_{ij} \geq r_{\mathrm{C}} \end{cases} \tag{2}$$

where a_{ij} is an interaction parameter between beads i and j, r_{C} is the cut-off radius, $\mathbf{r}_{ij} = \mathbf{r}_i - \mathbf{r}_j$, $r_{ij} = |\mathbf{r}_{ij}|$, $\hat{\mathbf{r}}_{ij} = \mathbf{r}_{ij}/|\mathbf{r}_{ij}|$. The a_{ij} and r_{C} values for each bead pair are obtained from Anderson *et al.* (2018)[36].

The forces $\mathbf{F}_{ij}^{\mathrm{D}}$ and $\mathbf{F}_{ij}^{\mathrm{R}}$ are given by

$$\mathbf{F}_{ij}^{\mathrm{D}} = -\gamma\omega^{\mathrm{D}}(r_{ij})(\hat{\mathbf{r}}_{ij} \cdot \mathbf{v}_{ij})\hat{\mathbf{r}}_{ij}, \tag{3}$$

$$\mathbf{F}_{ij}^{\mathrm{R}} = \sigma\omega^{\mathrm{R}}(r_{ij})\zeta_{ij}\hat{\mathbf{r}}_{ij}\Delta t^{-1/2}, \tag{4}$$

where ω^{D} and ω^{R} are distance-dependent weight functions that vanish for $r_{\mathrm{C}} < r$, γ is a friction coefficient, σ is the noise amplitude, $\mathbf{v}_{ij} = \mathbf{v}_i - \mathbf{v}_j$, $\zeta_{ij}(t)$ is a randomly fluctuating Gaussian variable, with zero mean and unit variance.

It was shown[37] that one of the weight functions, can be chosen arbitrarily and this fixes the other weight function, in order to satisfy the fluctuation-dissipation theorem. The relationship between the two functions is

$$\omega^{\mathrm{D}} = [\omega^{\mathrm{R}}]^2 \tag{5}$$

and the relationship between amplitudes

$$\sigma^2 = 2\gamma k_{\mathrm{B}}T, \tag{6}$$

where k_{B} is the Boltzmann constant and T is the temperature These two forces together form a thermostat, maintaining the temperature of the system. The function used for ω^D is

$$\omega^{\mathrm{D}} = \begin{cases} (1 - \frac{r_{ij}}{r_{\mathrm{C}}})^2 & \text{for } r_{ij} < r_{\mathrm{C}}, \\ 0 & \text{for } r_{ij} \geq r_{\mathrm{C}}. \end{cases} \tag{7}$$

To bond beads together to form long chain molecules, two additional forces are introduced to Eq. 1. The first is a simple harmonic spring force

$$\mathbf{F}_{ij}^{\mathrm{S}} = \sum_j C(r_{ij} - l_0)\hat{\mathbf{r}}_{ij}, \tag{8}$$

where the sum runs over all of the beads which are directly connected (*i.e.* those which are chemically bonded) to bead i. $C = 150$ (DPD units) is the spring constant and l_0 is an unstretched bond length. Bond lengths are set according to the number of heavy atoms[36] n_i and n_j in the bonded beads, calculated as $l_0 = 0.1(n_i + n_j) - 0.01$.

A further bonding force takes into account the molecular stiffness, where the potential defining this force is

$$U = \frac{1}{2}K(\theta - \theta_0)^2 \tag{9}$$

where the angle θ is defined as the scalar product of the two bonds connecting beads $i-1$, i and i, $i+1$ (in other words the angle between adjoining bonds), $K = 5$ (DPD units) is a bending constant, and $\theta_0 = 180°$ is a preferred, equilibrium angle.

Finally, to model the electrostatic pair potential between charged beads, we use Slater-type charge smearing, where the potential U_{E} between two charged beads i and j is given by

$$U_{\mathrm{E}} = \frac{\Gamma q_i q_j}{4\pi r_{ij}}[1 - (1 + \beta^* r_{ij})e^{-2\beta^* r_{ij}}] \tag{10}$$

where q_i and q_j are the charges, $\Gamma = e^2/(k_{\mathrm{B}}T\epsilon_0\epsilon_r r_{\mathrm{C}})$ is a dimensionless electrostatic coupling parameter, and $\beta^* = 0.929 r_{\mathrm{C}}^{-1}$ is the tuneable Slater parameter.

2. Thermostatting

DPD does not require a thermostat to maintain the temperature of the system, instead using the dissipative and random forces to control the temperature. The dissipative force parameter γ can be used to alter the dynamic viscosity μ of the simulated fluid. However, the relationship between γ and μ in DPD is fairly complex[38]. Furthermore, standard choices for parameters in $\mathbf{F}_{ij}^{\mathrm{D}}$ and $\mathbf{F}_{ij}^{\mathrm{R}}$ lead to a viscosity which is extremely low compared to what is expected for real fluids. Similarly, the mass diffusivity is also too high, and this (combined with low viscosity) generates a fluid with an unrealistically small Schmidt number (on the order of ≈ 1). This low Schmidt number is suitable for gases, but too small for liquids (≈ 1000). Since using standard DPD alone it is difficult to simulate a realistic fluid viscosity and Schmidt number, we apply the Stoyanov-Groot[39] external pairwise thermostat during viscosity calculations. This also allows us to vary the Schmidt number to investigate its influence on the results.

The Stoyanov-Groot thermostat was specifically developed for DPD particle systems and is a combination of the Lowe-Anderson[40] thermostat and a thermostat which is similar to the Nosé-Hoover[41] thermostat, coupled in parallel. The thermostat works by selecting pairs of beads and altering their velocity after each time step. The velocity is altered such that the temperature of the system is maintained. For each pair of beads that is selected, we choose between the Nosé-Hoover thermostat and the Lowe-Anderson thermostat with probability $P = \Gamma\Delta t$ (where Δt is the integration time step and Γ an exchange frequency). The resulting fluid viscosity is linearly proportional[39] to the choice of parameter Γ, while diffusivity $D \propto 1/\Gamma$, meaning that Schmidt number $\mathrm{Sc} \propto \Gamma^2$. When the switching probability P is low, the Nose-Hoover thermostat dominates, producing a fluid with a high diffusion coefficient and low viscosity. When P is high the Lowe-Anderson thermostat dominates, producing a fluid with low diffusion and high

viscosity. Switching between the two (in the form of the Stoyanov-Groot thermostat) allows us to vary the Schmidt number easily and significantly.

3. Geometrical Size of Micelles and Molecules

The radius of gyration, R_{G} is used to quantify the size and shape of micelles. This is calculated using

$$R_{\mathrm{G}}^2 = \frac{1}{N_{\mathrm{M}}} \sum_{k=1}^{N_{\mathrm{M}}} (\mathbf{r}_k - \mathbf{r}_{\mathrm{M}})^2 \tag{11}$$

where $\mathbf{r}_k$ is the position of a particle in a micelle consisting of N_{M} beads and $\mathbf{r}_{\mathrm{M}}$ is the centre-of-mass for the micelle $\mathbf{r}_{\mathrm{M}} = \sum_i^{N_{\mathrm{M}}} m_i \mathbf{r}_i / \sum_i^{N_{\mathrm{M}}} m_i$. Similarly, the size and shape of individual molecules are also quantified using their radius of gyration R_{g} (note the variation of subscript for the radius of gyration of molecules R_{g} vs. that for the whole micelle R_{G}). This is defined as the average squared distance of the beads making up the molecule, from its centre of mass. Therefore, for a single molecule

$$R_{\mathrm{g}}^2 = \frac{1}{N_{\mathrm{S}}} \sum_{k=1}^{N_{\mathrm{S}}} (\mathbf{r}_k - \mathbf{r}_{\mathrm{S}})^2, \tag{12}$$

where N_{S} is the number of particles in the surfactant molecule and r_{S} is the centre-of-mass for the surfactant molecule.

B. Shear Flow and Viscosity

1. Equilibrium methods

A typical method for calculating viscosity in molecular simulations uses Green–Kubo relations[42,43], using the auto-correlation function (ACF):

$$\eta = \frac{V}{k_{\mathrm{B}}T} \int_0^\infty \langle \sigma_{\alpha\beta}(t_0) \sigma_{\alpha\beta}(t + t_0) \rangle_{t_0} dt \tag{13}$$

where $\sigma_{\alpha\beta}$ are the off-diagonal components of the stress tensor, α and β represent the x, y, and z directions and V is the simulation volume. Angular brackets indicate an average over different time origins t_0. While the stress tensor consists of nine components $\sigma_{\alpha\beta}$ defining the state of stress at a point inside the simulation box, only the off-diagonal components are required for calculating the viscosity. Since $\sigma_{\alpha\beta} = \sigma_{\beta\alpha}$, there are three unique off-diagonal components. For isotropic phases, only integration over one of these stress tensor components is required to calculate η, since all off-diagonal components should produce equivalent values for the viscosity. This integrand decays to zero in the limit of a long t, in practice, the integration is usually performed up to time t_{C}, beyond which the integrand is negligible. This method calculates a viscosity without the application of shear and therefore calculates a zero-shear viscosity. Therefore, it is most commonly used for Newtonian fluids where the viscosity is independent of the shear rate.

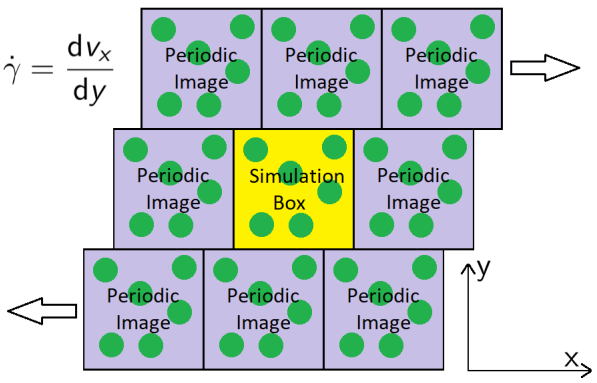

FIG. 2: Illustration of Lees-Edwards boundary conditions[44] for shear flow. The shear rate $\dot{\gamma}$ is calculated using the velocity v_x of the box.

2. Non-equilibrium methods

In order to investigate fluids which are expected to exhibit non-Newtonian behaviour, a non-equilibrium approach should be taken. In this work, we used Lees-Edwards boundary conditions[44], which are an adaptation of standard periodic boundary conditions for inducing shear flow. The theoretical implementation of these boundary conditions is illustrated in Fig. 2. Domains which are periodic to the simulation box are given a velocity which is proportional to their vertical position (relative to the simulation box). As a bead in the simulation box moves through the boundary at either the top or the bottom of the domain, its velocity and tangential position change as a result, generating a linear velocity profile over the simulation box domain. We note that it has been shown that Lees-Edwards boundary conditions for DPD can display non-physical jumps in the velocity profiles[45,46]. However, this behaviour only manifests at high dissipation rates (drag coefficient γ in Eq. 3) and is due to the velocity dependence of the DPD thermostat. In this work we see no unnatural jumps in the velocity profiles for the value of γ used and for the values of shear rate used.

For an isotropic fluid, such as micellar solutions, the shear viscosity can be simply calculated using the stress tensor $\sigma_{\alpha\beta}$ and the applied shear rate $\dot{\gamma}$. For a shear flow defined by velocity field $\mathbf{v} = v_x(y)\hat{\mathbf{x}}$, there is only one non-zero off-diagonal component of the stress tensor: σ_{xy} (or the equivalent σ_{yx}). The shear rate is calculated as $\dot{\gamma} = \partial v_x / \partial y$, therefore the viscosity is calculated by

$$\sigma_{xy} = -\eta \frac{\partial v_x}{\partial y}. \tag{14}$$

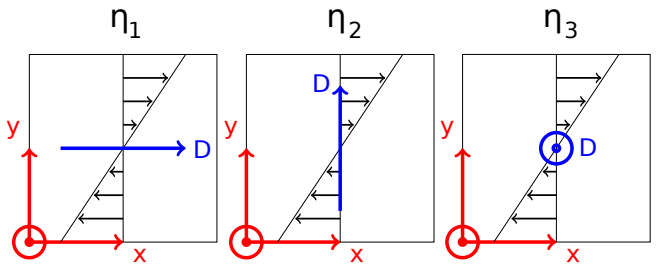

FIG. 3: Definition of Miesowicz viscosity coefficients η_1, η_2, and η_3. Measurement of the coefficients η_i involved orientating the director of the liquid crystal $\mathbf{D}$ relative to the flow velocity.

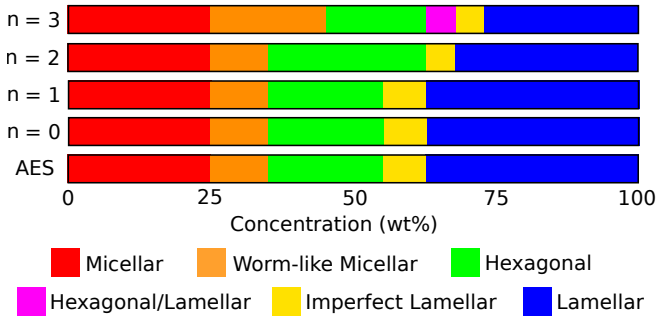

FIG. 4: Equilibrium phase diagrams for varying degrees of ethoxylation n, originally presented in Hendrikse *et al*[1].

The stress tensor is calculated using the Irving-Kirkwood definition[47], by summing components of pairwise forces and vectors between bead pairs. This is calculated as

$$\sigma_{\alpha\beta} = \sum_i (m_i v_{i,\alpha} v_{i,\beta} + \sum_{j>i} F_{ij,\alpha} r_{ij,\beta}), \qquad (15)$$

where the sum is over all beads i in the system (although, as noted above, only the component defined by $\alpha = x$ and $\beta = y$ is needed to calculate the viscosity). Averaging the value calculated over a large number of time steps allows us to find an accurate value for η.

However, for a nematic or a smectic liquid crystal, there can be considered to be three different shear viscosity coefficients, depending on the direction of shear flow relative to director $\mathbf{D}$. Miesowicz viscosity coefficients η_1, η_2, or η_3 are defined from the shear viscosities when the director lies along the x, y, or z axis, respectively (see Fig. 3). A summary of the three viscosities in relation to the flow velocity $\mathbf{v}$ follows[48]:

- η_1 is when director $\mathbf{D}$ is parallel to flow velocity;
- η_2 is when $\mathbf{D}$ is parallel to the velocity gradient;
- η_3 is when $\mathbf{D}$ is orthogonal to both the flow and the velocity gradient.

III. SIMULATION SET-UP

The DPD phase structures for SLES solutions are reported in previous works[1], where it was observed the micellar and lamellar phases spontaneously form under equilibrium conditions, while the formation of hexagonal phases requires a small amount of shear to be applied to encourage equilibration. In this work we initialise our simulations at concentrations across the phase diagram, using the pre-equilibrated phases from our previous work, where the equilibrium phase diagram is summarised in Fig. 4.

Simulations are performed for cases with different degrees of ethoxylation, where we vary the number of ethylene oxide groups in the range $0 \leq n \leq 3$. We also simulate a case with a distribution of n (in order to replicate the distribution that would be found in a commercial product) with an average $\bar{n} \approx 1$, which we refer to in this work as AES. Our simulated AES is made up of: $n = 0$ (52.7 wt.%), $n = 1$ (25.8 wt.%), $n = 2$ (14.0 wt.%), and $n = 3$ (7.5 wt.%).

A. Micellar Solutions

For micellar solutions, we take two approaches to calculating the viscosity. The first is using the stress tensor auto-correction function, and the second is via the application of shear. In both cases, the Stoyanov-Groot thermostat is used. Using the equilibrium approach, a selection of collision parameter values are trialled ranging from $\Gamma = 0$ (*i.e.* a pairwise variation of the Nosé-Hoover thermostat) to $\Gamma = 250$. The time step $\Delta t = 0.01$ is used for all micellar calculations.

When shear is applied, we trial different shear rates varying from $\dot{\gamma} = 1.2 \times 10^{-6}$ to $\dot{\gamma} = 1.2 \times 10^{-1}$ (DPD units). While there are different approaches to the conversion of DPD units to SI units, one common method for converting the time scale of DPD simulations results from matching the energy $k_B T$, to the experimental value at room temperature. This results in an estimate for the time scale of $\tau_C = 2.16 \times 10^{-12}$ s (see appendix A for details). This means that the shear rate $\dot{\gamma} = 1$ in DPD units converts to SI units of $\dot{\gamma} = 4.61 \times 10^{11}$ s^{-1}. Since rheometer measurements are typically[1] conducted at around $\dot{\gamma} \approx 10^{-3} - 10^{3}$ s^{-1}, the usual shear rates used in simulations are very large. One of the main barriers to achieving lower shear rates is the noise-to-signal ratio in the stress tensor.

For pure water at 25°C, experimentally determined values for the self-diffusion coefficient and the viscosity find a Schmidt number of approximately Sc ≈ 400. This means that an equivalent Schmidt number in DPD would be generated with a collision parameter of $\Gamma \approx 45$ (see appendix B), which is the primary value we use for these calculations. In addition, we perform simulations using $\Gamma = 250$, in order to investigate whether the Schmidt number has any influence on the behaviour of micelles

under shear and the quantities that we calculate.

B. Lamellar and Hexagonal Phases

Lamellar and hexagonal phases are expected to show shear-thinning behaviour, and therefore the autocorrelation function method is not appropriate for determining their viscosity. Instead, we perform simulations to study the behaviour of the liquid crystal phases under the application of shear. Lyotropic liquid crystals typically have very high viscosity values[1] and very low values of diffusion. The water self-diffusion coefficient in micellar solutions typically takes a value which is close to that of water self-diffusion in pure water[49] (2.3×10^{-9} m^{2}s^{-1} at 25°C[50]). In contrast, the water self-diffusion in liquid crystals is typically measured to be up to an order of magnitude smaller[49,51]. Similarly, the self-diffusion coefficient for the surfactant molecules can be up to two (or greater) orders of magnitudes smaller in the liquid crystalline phases vs. the micellar solutions[49,52].

The effect of higher viscosity and lower diffusion coefficient generates an even larger value of the Schmidt number, although due to the non-Newtonian nature of the liquid crystals it is not possible to obtain an exact value. For these cases, we chose to simulate using collision parameter $\Gamma = 250$, which requires a lowering of the time step to $\Delta t = 0.001$. This choice of Γ generates a Schmidt number for water beads of $\approx 10,000$ (*i.e.* 25 times larger than in the micellar solutions using $\Gamma = 45$). This value is selected due to it being one of the largest Schmidt numbers obtainable, without having to further lower the time step (see appendix B).

Experimentally, both the hexagonal[27–30] and lamellar[31–34] phases have been shown to exhibit phase orientation under the application of shear. For a lamellar phase, there is generally a preference to orientate in either the parallel or perpendicular orientation (see Fig. 5), while the hexagonal rods at low temperatures tend to align in the direction of shear flow (see Fig. 6).

In order to form a perfect parallel or perpendicular arrangement of lamellar layers under the application of shear (*i.e.* an arrangement such that the lamellar layers are parallel with one of the cubic box surfaces), the box size L should be chosen to be an integer multiple of the equilibrium d-spacing. If a non-integer box size is chosen, then the layers can form at diagonal orientations, even under the application of shear. This is likely to be because the potential energy benefit of forming at the correct d-spacing value is greater than the impact of shear. The equilibrium d-spacing was reported in previous works[1], calculated in boxes of size $L = 40$. For the $n = 0$ with $c = 70$ wt.% case, the equilibrium d-spacing is reported as $d = 5.71$, and an integer number of lamellar layers are formed by a box of size $L = 40$ (7 layers). Additional simulations are conducted for the $n = 1$ and AES distribution of n at 70 wt.%, where we use a box size of

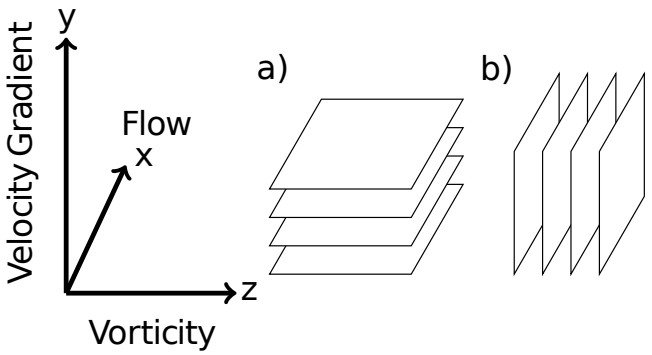

FIG. 5: Lamellar layers which are stacked in a) the direction of the velocity gradient (parallel orientation) and b) those which are stacked along the velocity gradient-neutral plane (perpendicular orientation). Both orientations can form under the application of a shear force.

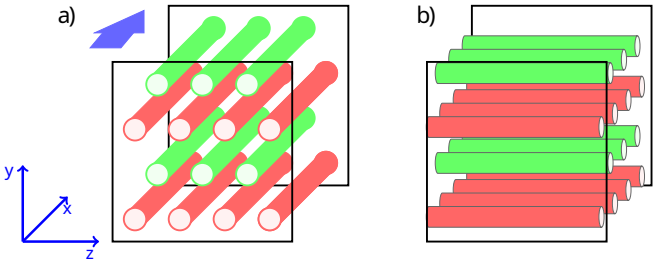

FIG. 6: When shear flow is induced (here in the x-direction as indicated by the blue arrow), the rods in the hexagonal phase align in either in (a) an in-shear-plane or (b) an out-of-shear-plane (log-rolling) orientation.

$L = 39$ for $n = 1$ (equilibrium d-spacing value $d = 6.49$ producing 6 layers) and $L = 25$ for AES (equilibrium d-spacing value $d = 6.32$ producing 4 layers). Shear is applied so that the flow velocity is directed along the x axis and a linear velocity profile is generated along the y-axis.

IV. RESULTS AND DISCUSSION

A. Viscosity of micellar solutions

In this section, we calculate the viscosity using the autocorrelation method (Eq. 13), where no external shear force needs to be applied for the calculation. Data acquisition of the stress tensors σ_{xy}, σ_{xz} and σ_{yz} occurs after the micellar simulation boxes are equilibrated (i.e. after they have reached an equilibrium number of micelles as quantified in previous work[1]). The equilibrium aggregation numbers for different micellar solutions are given in Table I, where we reported that the aggregation numbers are under-predicted when compared with

	$c = 7$ wt.%	$c = 10$ wt.%	$c = 20$ wt.%
$n = 0$	40	52	75
$n = 1$	37	44	88
$n = 2$	38	50	87
$n = 3$	36	47	77
AES	43	53	85

TABLE I: Final mean aggregation number N_{agg} for micellar solutions of varying concentration c and degree of ethoxylation n.

experimental results. For example, experimentally the the mean aggregation number of SDS solutions ($n = 0$) at concentrations 10 wt.% possess aggregation numbers $N_{\text{agg}} = 104 - 108$[53,54], and similarly at higher concentrations $N_{\text{agg}} = 104 - 112$[53,55]. This means that the aggregation numbers at 10 wt.% and 20 wt.% in DPD are around ≈ 50 wt.% and ≈ 70 wt.% of the experimental values, respectively.

The aggregation number is calculated as a number average, and therefore N_{agg} is defined as the mean number of molecules per micelle. Molecules are defined as being in the same aggregate when the distance between their tail beads is less than a defined cut-off $r_{\text{c-off}}$ which we chose as $r_{\text{c-off}} = r_{\text{C}} = 1$. Only one tail bead pair distance must be less than this cut-off for them to be defined as belonging to the same micelle.

For the calculation of viscosity, one must apply a cutoff in Eq. 13, for which to integrate over time t. We choose the cutoff $t_{\text{C}} = 1.8$ for all simulation cases for consistency, at a value at which all auto-correlation functions have decayed to approximately zero. Fig. 7 shows the viscosity for solutions with varying concentration, when collision parameter $\Gamma = 0$ is used (for reference the viscosity of water obtained using $\Gamma = 0$ is $\eta = 0.70$). The viscosities for different ethoxylation values n are very similar, with no trend in n being observable due to overlapping error bars. However, there is a clear growth in the viscosity with increasing concentration. The rate of growth with concentration is, however, at a reduced rate when compared with what is expected from experimental measurements[3]. This could partially be explained by the under-prediction of the aggregation number in the simulations since there is evidence that the viscosity increases with increasing aggregation number.

While $\Gamma = 0$ produces an unrealistically low Schmidt number for fluids, the autocorrelation function decays as a function of time more slowly when Γ is small. Therefore for low Γ values, it is easier to find a value for the viscosity. It was found that at larger Γ values, the autocorrelation function decayed too quickly to calculate precise viscosity values (see Appendix C for more details).

However, we investigate the impact which Γ has on the molecular radius of gyration R_{g}. The radius of gyration is found to be independent of the collision parameter Γ for all simulation cases of n and concentration c. An example of this for one simulation case is shown in Table II. This is in agreement with previous DPD work for polymers[25]. Therefore we conclude from these calculations that although the choice of Γ does not necessarily lead to a physically meaningful value for the Schmidt number, the DPD simulated results under equilibrium are not particularly sensitive to it. Following this, we now investigate whether this is also true for micellar solutions which are not under equilibrium conditions when shear is applied.

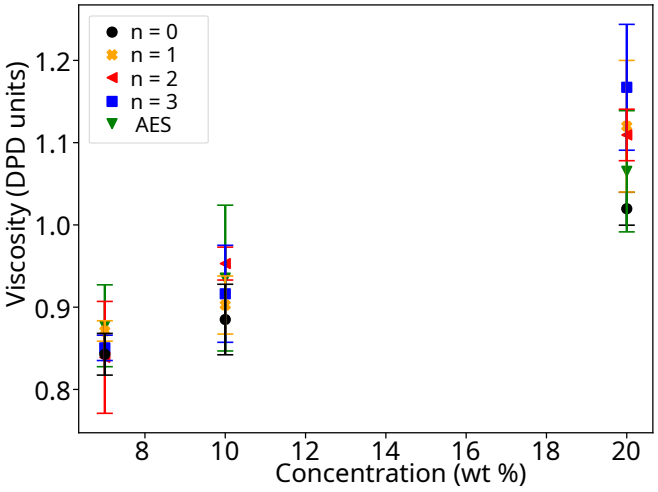

FIG. 7: Viscosity of micellar solutions using the autocorrelation method ($\Gamma = 0$). The error bars represent the standard deviation of the values obtained from different off-diagonal stress tensor components.

Thermostat parameters	Radius of gyration R_{g}
$\Gamma = 0$	0.8541 ± 0.0007
$\Gamma = 10$	0.8548 ± 0.0006
$\Gamma = 45$	0.8546 ± 0.0005
$\Gamma = 250$	0.8543 ± 0.0005

TABLE II: Average R_{g} for micellar solutions with $n = 0$ and $c = 20$ wt.% when collision parameter Γ is varied. The uncertainties represent the standard deviation over the data acquisition period.

B. Micellar solutions under shear

In this section, we study the impact that shear has on the micelles and the calculated viscosity. Simulation cases investigated include when $n = 0$ (10 wt.% and 20 wt.%), $n = 1$ (10 wt.% and 20 wt.%) and AES (10 wt.% and 20 wt.%). We first present the impact of shear rate on the micellar shape and the impact this has on the molecules, before calculating the viscosity as a function of shear rate. Figs. 8 and 9 show examples of micellar solutions under shear for two different collision parameters $\Gamma = 45$ and $\Gamma = 250$, which will be analysed in this

section.

1. Micellar Shape

a. Collision parameter $\Gamma = 45$. When the shear rate is low ($\dot{\gamma} \leq 1.2 \times 10^{-4}$) there is little change in micellar shape compared with equilibrium simulations. However, at high shear rates $\dot{\gamma} \geq 1.2 \times 10^{-3}$ changes in shape are observed, as illustrated in Fig. 8.

At higher shear rates longer, and more worm-like micelles become aligned in the direction of the shear flow. An increase to $\dot{\gamma} = 1.2 \times 10^{-2}$ causes micelles to noticeably elongate in the direction of shear flow. Finally, an increase to $\dot{\gamma} = 1.2 \times 10^{-1}$ breaks down the micelles into a nematic phase. This abrupt change occurs at the same shear rate for all concentrations and ethoxylation values simulated.

The shape and aggregation number N_{agg} has a significant impact on the micellar radius of gyration R_{G}, as shown in Fig. 10. Moderate amounts of shear slightly enhance the aggregation number, by encouraging free molecules to join aggregates. Once the micelles start to significantly stretch, they break into smaller aggregates, decreasing the mean aggregation number. The radius of gyration R_{G} grows significantly under shear, mostly due to the stretch of the micelles; once they break down into smaller aggregates at high shear rate, R_{G} drops accordingly. Both the 10 wt.% and 20 wt.% concentrations show similar trends with increasing shear rate.

Fig. 11 shows the impact of shear rate on the radius of gyration of the individual molecules R_{g}, with the effects most pronounced when micelles have completely broken down. It might be expected that R_{g} would increase with shear rate due to stretching, however, the opposite trend is found.

b. Collision parameter $\Gamma = 250$. The impact of shear on the $n = 1$ with 20 wt.% concentration case is shown in Fig. 9 (equivalent to the case in Fig. 8 with $\Gamma = 45$), and we observe the same transition from spherical micelles to work-like micelles, followed by a breakdown of micellar structure. Increasing the value of Γ is, however, found to lower the value of the shear rate at which the transition from spherical micelles to stretched micelles occurs. Therefore disaggregation also occurs at a lower shear rate.

The impact of Γ on the mean aggregation number and radius of gyration of micelles is shown in Fig. 12. There is relatively little difference between the two choices of Γ at lower shear rates. Some slight differences begin to appear at higher shear rates, although this is likely to be related to the transition from non-spherical micelles occurring at a lower shear rate when $\Gamma = 250$.

It was shown in the previous section, that varying the collision parameter Γ had minimal effect on the radius of gyration of molecules R_{g} when no shear is applied. The variation of R_{g} with shear rate, for both values of Γ trialled, is shown in Fig. 13. The radius of gyration displays very different behaviour at extremely high shear rates when the micelles have largely broken down, indicating that the choice of Γ has more of an influence on the individual molecules than it does on micelles. Symeonidis *et al.*[25] reported for polymer systems that the radius of gyration of molecules grows with increasing shear rate, irrespective of Γ. An increase in R_{g} with shear rate has been observed in simulations by other authors[56], as well as theory[57] and experiment[58]. This increase can be explained by a stretch of the molecule. In our case, the radius of gyration does indeed increases when $\Gamma = 250$, at shear rates when micelles have largely been broken down ($\dot{\gamma} > 1.3 \times 10^{-3}$). However, we find that when $\Gamma = 45$, the radius of gyration decreases at high shear rates. This decrease coincides with micelle breakdown ($\dot{\gamma} > 1.3 \times 10^{-2}$). This decrease could be explained by the fact that micelle formation has been shown to increase the radius of gyration[59]. We believe that there are two competing factors influencing R_{g}, and there is a competition between the influence of the shear rate and phase structure.

2. Viscosity Calculation

Eq. 14 is used to calculate the viscosity when shear is applied. It is found that there is too much noise in the stress tensor when $\dot{\gamma} < 1.2 \times 10^{-4}$ in order to obtain a converged value for viscosity. Therefore Fig. 14 shows the viscosity calculated at higher shear rates for varying concentrations and degrees of ethoxylation.

We observe a shear thinning behaviour, which is related to the change in the micellar shape and their breakdown. As discussed in section III A, the shear rates used are high when compared with those used in typical experiments. This explains why we do not see a Newtonian relationship, since the shear rates used in experiment are unlikely to lead to any micellar breakdown or shape changes, like the ones observed in simulation.

Due to the difficulty in accessing lower shear rates, it can't be determined if the viscosity eventually plateaus to a Newtonian relationship with the shear rate at lower shear rate values (*i.e.* in the region in which the micelles are not thought to be changing shape). However, at the lowest shear rate value, the viscosity calculated for AES and $n = 1$ solutions at 20 wt.% is significantly larger than for when $n = 0$. This is in contrast with the 10 wt.% case where the viscosity calculated for $n = 0$, $n = 1$ and AES is more similar. The large difference in viscosity at 20 wt.% and minimal difference at 10 wt.% between n values is qualitatively consistent with experiment[1,3].

C. Orientation of liquid crystals

In this section, we consider the behaviour of higher concentration systems which form liquid crystal phases. We begin by performing experiments on simulation boxes

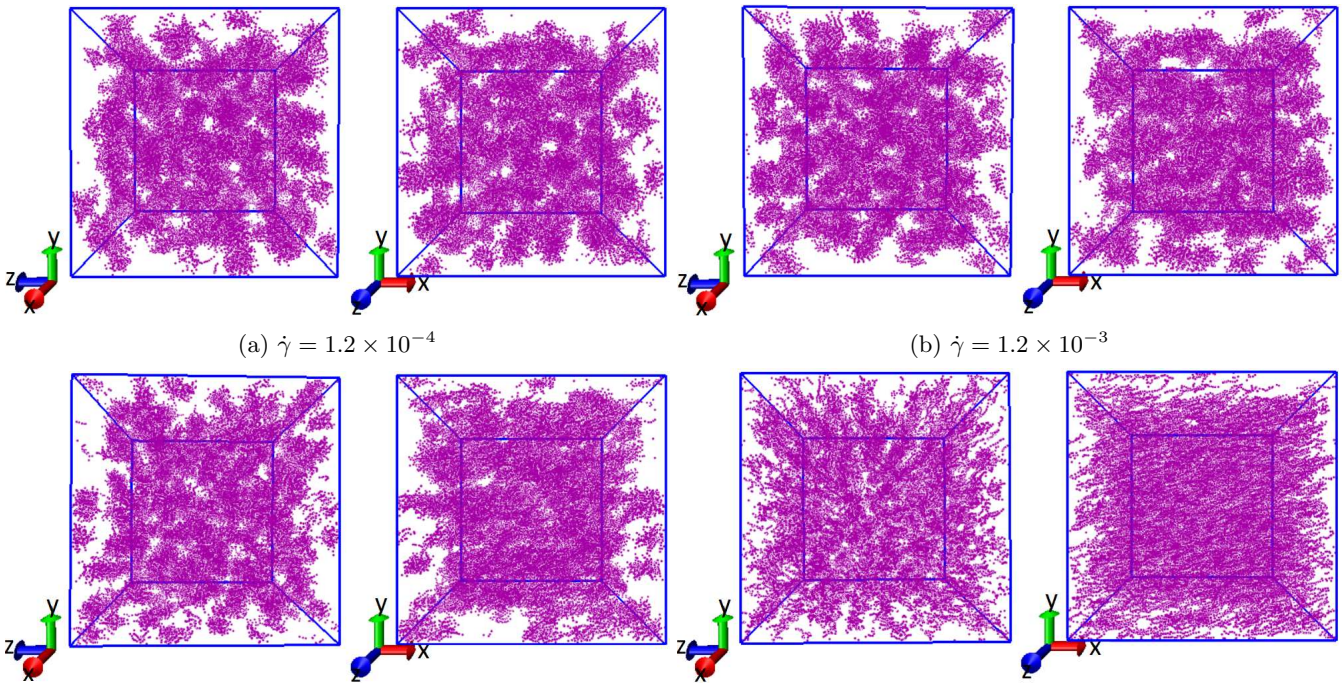

(a) $\dot{\gamma} = 1.2 \times 10^{-4}$ (b) $\dot{\gamma} = 1.2 \times 10^{-3}$

(c) $\dot{\gamma} = 1.2 \times 10^{-2}$ (d) $\dot{\gamma} = 1.2 \times 10^{-1}$

FIG. 8: A micellar solution ($c = 20$ wt.% and $n = 1$) at varying shear rates, where shear is applied in the x-direction. Note that only surfactant molecules are shown for clarity. Calculation performed using collision parameter $\Gamma = 45$.

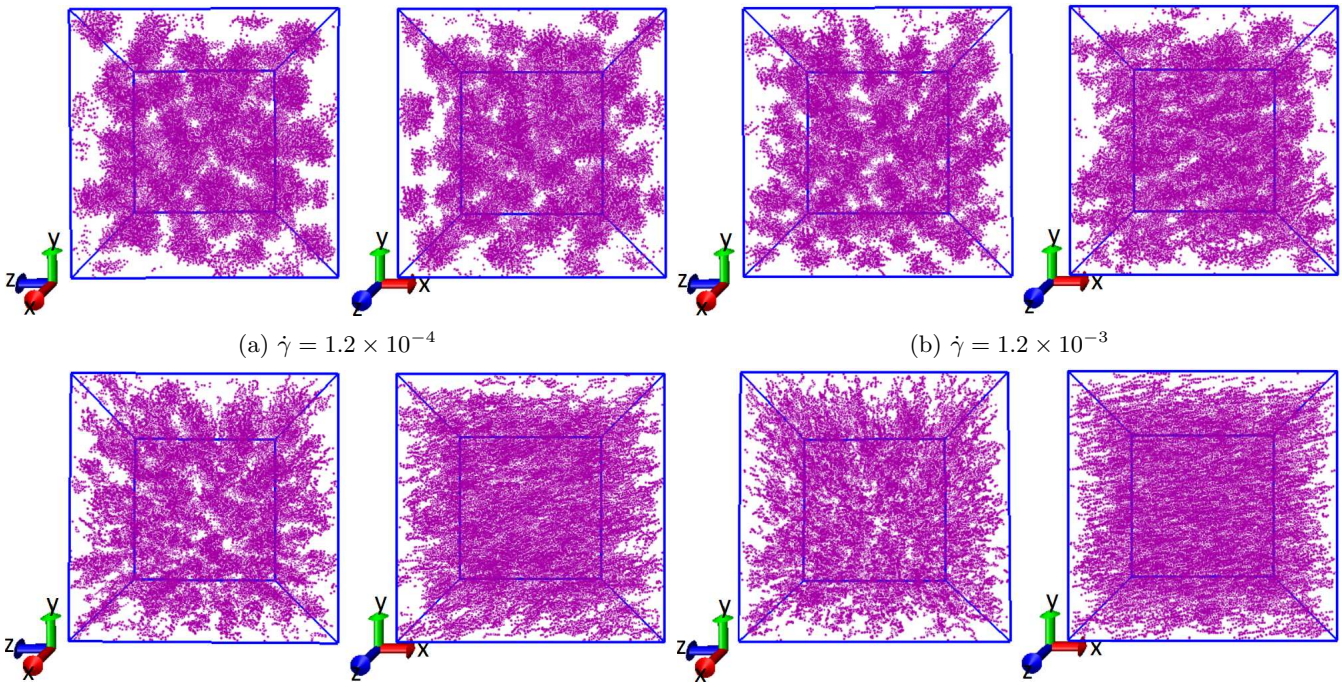

(a) $\dot{\gamma} = 1.2 \times 10^{-4}$ (b) $\dot{\gamma} = 1.2 \times 10^{-3}$

(c) $\dot{\gamma} = 1.2 \times 10^{-2}$ (d) $\dot{\gamma} = 1.2 \times 10^{-1}$

FIG. 9: A micellar solution ($c = 20$ wt.% and $n = 1$) at varying shear rates, where shear is applied in the x-direction. Note that only surfactant molecules are shown for clarity. Calculation performed using collision parameter $\Gamma = 250$.

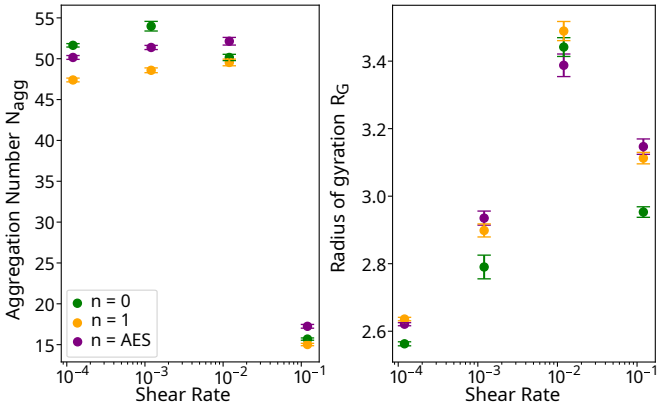

(a) $c = 10$ wt.%

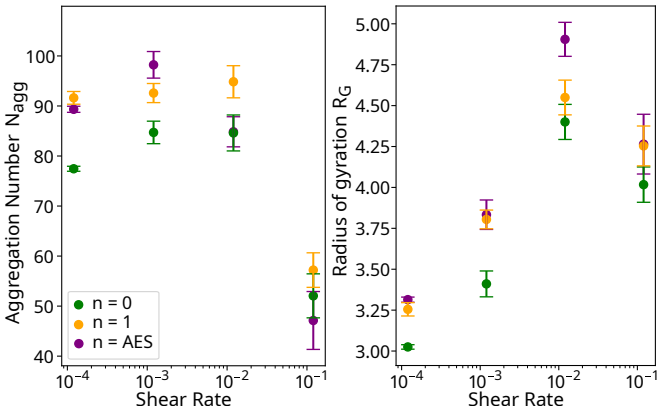

(b) $c = 20$ wt.%

FIG. 10: Effect of shear rate on the mean aggregation number N_{agg} and micellar radius of gyration R_{G}, for solutions with $n = 0$, $n = 1$, AES and concentrations $c = 10$ wt.% and $c = 20$ wt.%. Calculation performed using collision parameter $\Gamma = 45$.

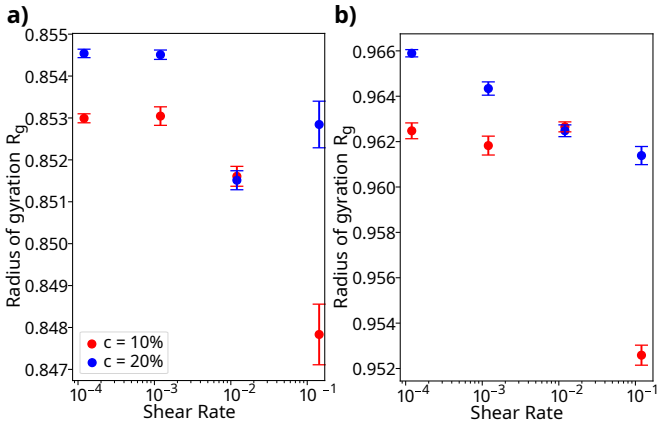

FIG. 11: Effect of shear rate on the radius of gyration R_{g} of molecules with a) $n = 0$ and b) AES. Calculation performed using collision parameter $\Gamma = 45$.

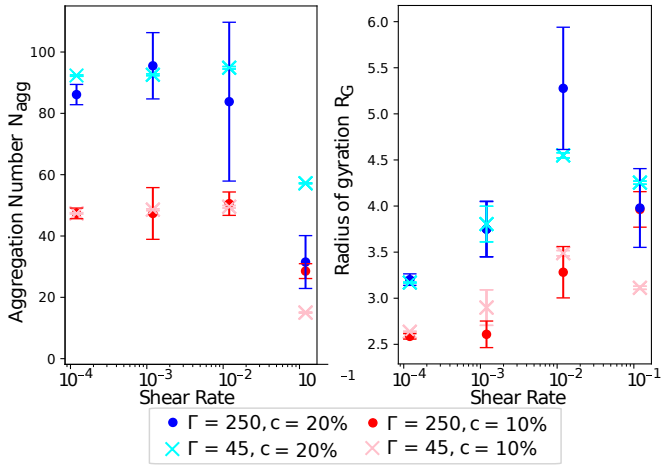

FIG. 12: Comparison of the values of N_{agg} and R_{G} obtained using different values of Γ. Results are shown for two different concentrations c and $n = 1$.

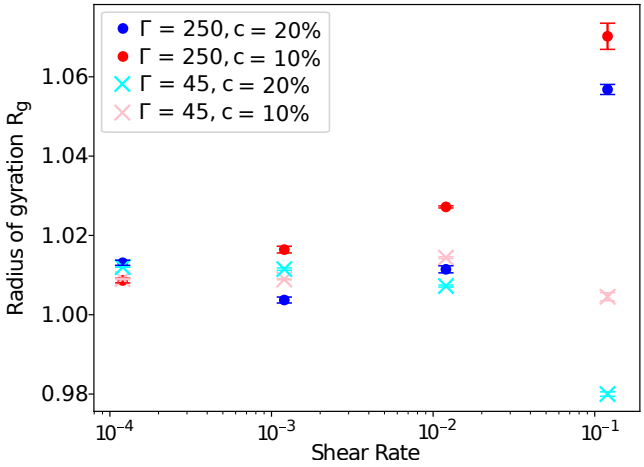

FIG. 13: Comparison of the values of R_{g} obtained using different values of Γ for molecules with $n = 1$. Results are shown for two different concentrations c.

with initially random placement of molecules, in order to determine the preferred orientation of the hexagonal and lamellar phases under shear. For lamellar phases, we investigate solutions with 70 wt.% concentration and observe that the lamellar layers orientate in the parallel orientation under shear $\dot{\gamma} \leq 6 \times 10^{-2}$ for all values of n trialled ($n = 0$, $n = 1$ and AES). This is consistent with experimental observations for SLES surfactants[2]. While it has been reported that some DPD simulations have shown transition from the parallel orientation at low shear rates, to the perpendicular phase at higher shear rates[60–62], this is not observed in this work. An increase to $\dot{\gamma} = 6 \times 10^{-1}$ leads to a breakdown of the parallel layers, and the system is no longer a lamellar phase. The phase most closely resembles a nematic liquid crystal phase at these high shear rates, due to the fact that although the lamellar layers have broken down and

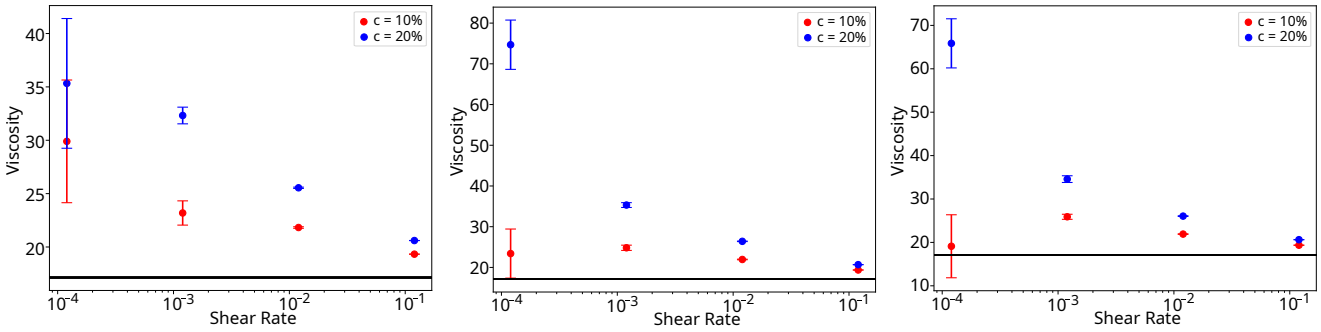

(a) $n = 0$ (b) $n = 1$ (c) AES

FIG. 14: Viscosity calculated at varying shear rates from applying shear in DPD calculations. Individual plots correspond to the ethoxylation n, while in each plot two different concentrations are shown. Error bars correspond to the standard error. The horizontal black line indicates the viscosity of water at a value of $\Gamma = 45$.

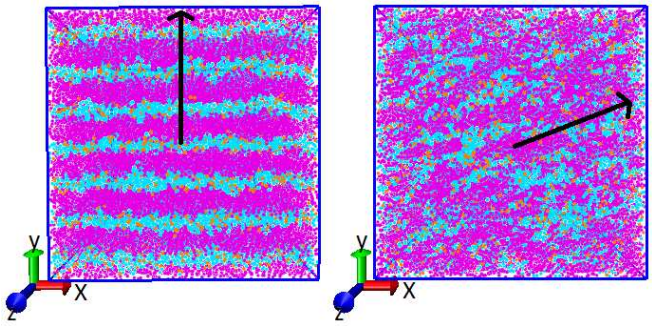

FIG. 15: Solution with $n = 0$ and $c = 70$ wt.% under shear, at $\dot{\gamma} = 6 \times 10^{-2}$ (Fig. a) and $\dot{\gamma} = 6 \times 10^{-1}$ (Fig. b). Flow velocity is in the x-direction and the velocity gradient the y-direction. An arrow represents the director and beads are coloured by: surfactant (pink), sodium ion (orange), and water (light blue).

there is now no positional order, the molecules still possess orientational order where molecules are parallel to each other. These two cases, along with the orientation of the director, are shown in Fig. 15.

For the lamellar phase, the director of the box is approximately defined as being in the direction parallel to the normal of the layers (along the y-axis). Upon transition into the nematic phase, the director aligns approximately along the direction of the shear flow (along the x-axis). The director vector is calculated as the average orientational vector for all surfactant molecules in the system, where the orientation vector is defined as the vector between the sulfate head bead and the final tail bead in each molecule. For the case shown in Fig. 15, the director for the nematic phase is calculated as (0.96, 0.29, 0), in other words, it is at an angle of 17° to the x-axis. The alignment of the director for a nematic crystal as parallel to the shear surface is in agreement with what is most commonly reported experimentally[63]. A selection of intermediate shear rates between $\dot{\gamma} = 6 \times 10^{-2}$ and $\dot{\gamma} = 6 \times 10^{-1}$ are trialled in order to investigate the possibility of an intermediate perpendicular orientation (at shear rates $\dot{\gamma} = 9 \times 10^{-2}$ and $\dot{\gamma} = 3 \times 10^{-1}$), however no evidence is found for the formation of a perpendicular phase.

For the hexagonal phase, we study concentrations of 40 wt.%, and it is found that when shear ($\dot{\gamma} = 6 \times 10^{-3}$) is applied to the simulation box, hexagonal rods lie in the in-shear-plane orientation, as described by Fig. 6. This orientation of the hexagonal phase is consistent with experiments for general surfactant systems[27–30].

D. Lamellar Viscosity

Since the lamellar phases in this work take the parallel orientation, calculating the viscosity would result in a calculation of the Miesowicz viscosity component η_2, as described by Fig. 3. Although we see no evidence of a natural transition to the perpendicular orientation of the lamellar layers, simulations can still be performed in order to investigate the viscosity component η_3 (perpendicular orientation). Since the perpendicular phase is not induced at any shear rate from an initially random configuration, this can be performed by taking a lamellar phase that is already in a parallel orientation, and rotating to the perpendicular, before undertaking the viscosity calculation. Some authors[34,35,60] have argued that the transition to this perpendicular phase occurs naturally, due to the perpendicular orientation having a lower viscosity than the parallel. A comparison of the calculated viscosity components η_2 and η_3, at high shear rates, is shown in Table III. Although a transition to the perpendicular orientation is not naturally observed at high shear rates, we do conclude that the viscosity calculated for the perpendicular orientation (η_3) is indeed lower than the parallel (η_2). This suggests that the transition from the parallel orientation to the perpendicular case is not entirely determined by the viscosity, and that other factors may influence the preferred orientation of the lamellar phase. It is of interest that it has been observed[31] that, in Cou-

Shear Rate	Perpendicular Viscosity	Parallel Viscosity
6×10^{-4}	178 ± 8	300 ± 10
6×10^{-5}	82 ± 10	206 ± 41

TABLE III: Comparison of the perpendicular and parallel viscosity (DPD units) for lamellar systems, calculated for two shear rates.

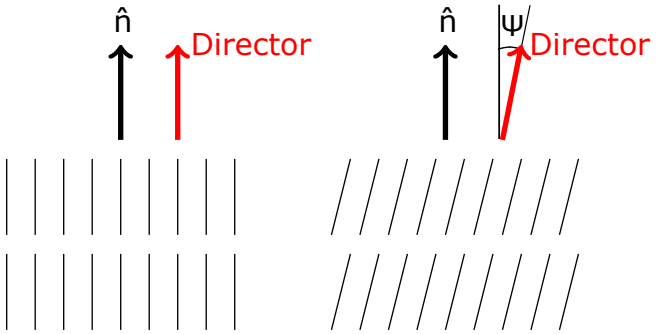

FIG. 16: Illustration of the orientation of the molecules under shear. The molecules retain their parallel layers, but are no longer parallel with the normal to the layer.

ette gap experiments, the orientation distribution is not always constant across the gap. In particular, there can be wall effects which result in a preferred parallel orientation at high shear rates.

E. Molecular changes to the Hexagonal and Lamellar phases

We now discuss the impact that shear has on the molecules in liquid crystal phases. While the structure of the phases is visually unchanged with varying shear rate (*i.e.* the shape and structure of the lamellar layers and hexagonal rods remains visually unchanged), the molecules may undergo stretching or shape changes within the layers as a result of the shear force.

Consider angle Ψ, which is defined as the angle between a normal to the lamellar layer surface $\hat{n}$, and the director of the surfactant molecules. This is illustrated in Fig. 16. Under shearing, the lamellar layers remain parallel to the $x-z$ plane, and therefore the normal to these layers remains as $\hat{n} = (0, 1, 0)$. The angle between the director and the normal of the layers is shown in Fig. 17, where the molecules rotate to an angle within the lamellar layers.

This movement has an effect on the molecular radius of gyration R_g, which is demonstrated in Fig. 17. While a significant amount of reorientation of the molecules is found for shear rates at $\dot{\gamma} = 6 \times 10^{-4}$, only a small amount of growth in the radius of gyration is found. When the shear rate increases to $\dot{\gamma} = 6 \times 10^{-3}$, the molecules significantly orientate themselves, and the molecules' stretch corresponds to a growth in the radius of gyration.

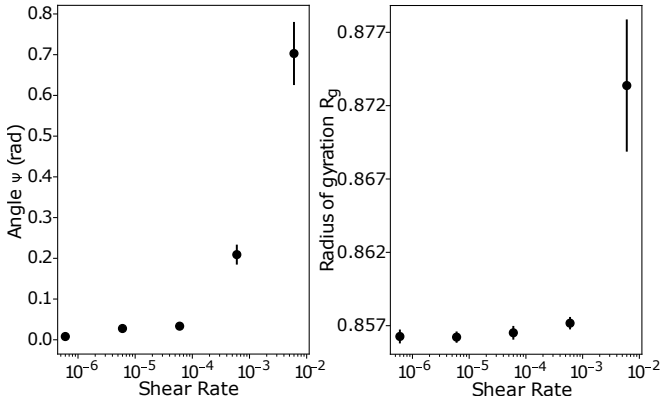

FIG. 17: Angle Ψ between the normal to the lamellar layers and the director of the surfactant molecules, as well as the radius of gyration, both as a function of shear rate for molecules in the lamellar phase with concentration $c = 70$ wt.% and $n = 0$.

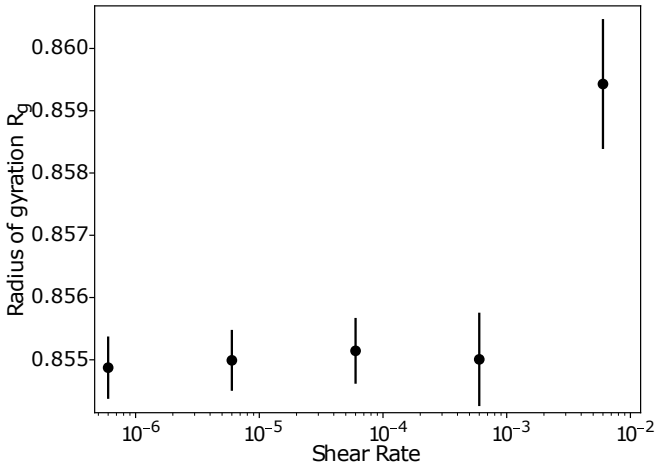

FIG. 18: The radius of gyration as a function of shear rate for molecules in the hexagonal phase with concentration $c = 40$ wt.% and $n = 0$.

At a shear rate of $\dot{\gamma} = 6 \times 10^{-2}$ (not shown in Fig. 17), the lamellar phase breaks down and the molecules no longer exist in parallel layers. Based on the rate of growth of angle Ψ in Fig. 17, the molecules at $\dot{\gamma} = 6 \times 10^{-2}$ would have angle $\Psi \approx 1.2$rad (linear extrapolation of the angle versus the log values corresponding to $\dot{\gamma} = 6 \times 10^{-3}$ and $\dot{\gamma} = 6 \times 10^{-4}$). This is likely to be a reason that the lamellar phase breaks down in the simulation box at this shear rate. A similar change in director orientation under shear has been reported in other simulation studies of the lamellar phase[34].

The radius of gyration for the hexagonal phase as a function of the shear rate is shown in Fig. 18. Similarly to the lamellar case, there is little change in the radius of gyration except at very high shear rates. Unlike the lamellar phase, the structure of the hexagonal phase is allowed more freedom to adjust its periodicity (inter-rod

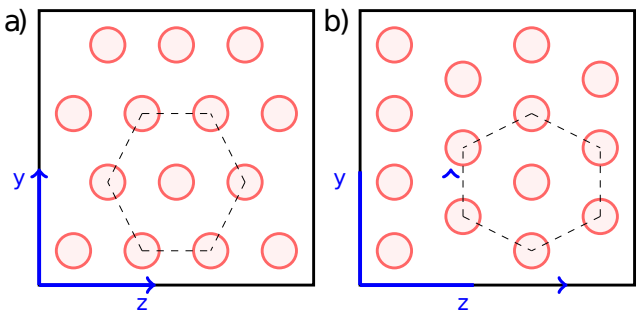

FIG. 19: If shear flow is induced in the x direction by shearing using the $x-z$ plane, rods in the hexagonal phase tend to align along the x-axis. The perpendicular plane ($y-z$ plane), experimentally, takes one of the two orientations that are given the name parallel (a) or perpendicular (b).

spacing r), since it can rotate in the y-z plane. It is found that at almost all values of increasing shear rate, there is no change in the value of its average inter-rod spacing r, until reaching a shear rate of $\dot{\gamma} = 6 \times 10^{-2}$. At this point r increases from $r = 7.52$ to $r = 7.85$. It was discussed in our previous work[1] that we observe a preference for hexagonal phases to orientate their unit cell in the y-z plane (as well rod alignment parallel to the x-axis), when subject to shear. In experiments, this is typically one of two orientations, as demonstrated in Fig. 19. In our simulation work, we observe a small preference for parallel orientations to form. However, the unit cell of the hexagonal phase is also restricted by the need to satisfy periodic boundary conditions, so perfect hexagonal lattices cannot form (that is, the unit cell is described by two vectors of different lengths) and the lattice must stretch in some way. Therefore, there is competition between the preference to forming a parallel orientation in the y-z plane, and forming a lattice which is as close to a perfect hexagonal lattice as possible. We believe the change in r we see at higher shear rates is due to this competition. The orientation of the phases when $r = 7.52$ is close to being in the parallel orientation, but not perfectly (there is a small angle between the z-axis and unit vector), while the $r = 7.85$ is a perfect parallel orientation (unit vector parallel to z). This indicates that the preference for forming parallel orientations strengthens at high shear rates, compared with the trade-off of a non-desirable inter-rod spacing.

V. CONCLUSION

In this work, we calculate the viscosity of micellar solutions using two different methods. Using an equilibrium approach we show that the viscosity of micellar solutions increases as a function of concentration, as is expected from experiment. We also show that the Schmidt number has no influence on the molecular radius of gyration when no shear is applied. Our second approach to calculating viscosity is a non-equilibrium one, and we apply shear using Lees-Edwards boundary conditions. Moderate shear rates mildly encourage the aggregation number to increase, by encouraging free surfactant molecules to join micelles. A typical problem encountered in DPD and other simulation methods is the under-prediction of the aggregation number[1,36]. Therefore, it is hypothesized that the equilibration of micellar systems can be encouraged by applying a small amount of shear during the micelle formation period, in order to increase the mean aggregation number towards values found experimentally.

We observe that at high shear rates, spherical micelles can stretch into worm-like micelles, stretching in the direction of shear flow. As a result of micellar breakdown, we observe a shear-thinning effect for micellar solutions. This is particularly important considering the large shear rates typically used in high-shear mixers, potentially leading to structural and viscosity changes during the manufacture of surfactant-containing products. We also show that the Schmidt number has a significant effect on the phase structure of micellar solutions under shear, including the radius of gyration. This is in contrast to what we find under equilibrium conditions. This is an important consideration for research comparing DPD simulations to real micellar solutions, given that standard DPD parameter choices result in unrealistic Schmidt numbers.

The lamellar and hexagonal phases are found to orientate relative to the direction of applied shear, in a way which is consistent with experiment. We find no evidence of a transition to a perpendicular phase at high shear rates for lamellar phases, despite the parallel phase having a higher viscosity. This is of interest since the transition to perpendicular phases is often explained by its lower viscosity alone.

For the lamellar layers, we apply shear by setting the box size based upon an integer multiple of the equilibrium d-spacing value. This allows us to ensure an integer number of lamellar layers between the two shearing planes. However, we assume that there is no change in the d-spacing value with varying shear rate. Experimentally, lamellar structures have been observed to exhibit changes in their d-spacing as a result of high shear rates[64,65]. However, it is rarely reported that there is a transition to a nematic phase where a breakdown of layers occurs. It is more often reported the parallel orientation persists at high shear rates[33], or that there is a transition to perpendicular orientations[31,32,35] or 'onions'[12] at high shear rates. Therefore it is possible that the lamellar layers should not disintegrate at high shear rate, as they do in the simulations (however no experimental data could be found in existing literature for SLES d-spacing under shear specifically). In the simulations, the disintegration is suspected to be due to the orientation of the molecules within the layers. The orientational change of the molecules would be expected to de-

crease the d-spacing by decreasing the thickness of the surfactant layer. However, due to the box size being chosen based on the equilibrium d-spacing, the spacing and thickness of the lamellar layers are unable to vary as a function of shear rate. This may mean that the thickness of the layers is forced to maintain an undesirable d-spacing value under the application of shear. It would be of interest in further work to investigate the effect of varying box size and lamellar spacing when subjecting lamellar phases to shear.

Finally, we show that the inter-rod spacing of the hexagonal phase can be altered depending on the shear rate applied. Hexagonal phases are typically difficult to form under equilibrium conditions in DPD simulations, so an approach to encouraging their formation is via the application of a small amount of shear[1,66]. Therefore, one must take care during this process that the shear rate chosen does not impact the resulting inter-rod spacing if the aim is to study the phase under equilibrium conditions.

AUTHOR DECLARATIONS

The authors have no conflicts to disclose.

ACKNOWLEDGMENTS

This work was supported by the Engineering and Physical Research Council (Grant number EP/L01615X/1). This work was performed using resources provided by the Cambridge Service for Data Driven Discovery (CSD3) operated by the University of Cambridge Research Computing Service (www.csd3.cam.ac.uk), provided by Dell EMC and Intel using Tier-2 funding from the Engineering and Physical Sciences Research Council (capital grant EP/T022159/1), and DiRAC funding from the Science and Technology Facilities Council (www.dirac.ac.uk). A significant proportion of the work presented was undertaken on ARC4, part of the High Performance Computing facilities at the University of Leeds, UK.

Appendix A: Converting DPD time scale to real units

Most work using DPD is usually presented in reduced DPD units, in which the unit of length is the particle size $r_\mathrm{C} = 1$, the unit of mass is the particle mass $m = 1$, and the unit of energy is defined by setting $k_\mathrm{B}T = 1$. One method of converting the units used in DPD to real units, is by matching the density of water in the simulation to a known experimental value, and therefore a value for r_C can be obtained in real units.

The parameterisation used in this work, presented by Anderson *et al.* (2018)[36], groups two molecules together to form the water bead in the simulation. Therefore, the mass of one DPD bead of water m is the mass of two water molecules; in real units, this is $m = 5.98 \times 10^{-26}$ kg. The number density ρ of beads in the simulation box is defined by $\rho r_\mathrm{C}^3 = 3$, which is a common choice for ρ across DPD literature due to the work of Groot and Warren[24]. The number density can be calculated as $\rho = \rho_\mathrm{m}/m$, where ρ_m is the mass density. Therefore combining relationships $\rho = \rho_\mathrm{m}/m$ and $\rho r_\mathrm{C}^3 = 3$ produces the following relation for r_C:

$$r_\mathrm{C} = \left(\frac{3m}{\rho_\mathrm{m}}\right)^{1/3}. \tag{A1}$$

Using that the density of water at room temperature is ≈ 1000 kg/m^3, this finds a value for r_C in real units to be $r_\mathrm{C} \approx 5.65 \times 10^{-10}$ m.

The temperature in the simulation is calculated using the velocity v using

$$\frac{1}{2}m\langle v^2\rangle = \frac{3}{2}k_\mathrm{B}T. \tag{A2}$$

By saying that the distance in real units $d_\mathrm{Real} = d_\mathrm{DPD}r_\mathrm{C}$; time in real units $t_\mathrm{Real} = t_\mathrm{DPD}\tau_\mathrm{C}$; and $v_\mathrm{DPD} = d_\mathrm{DPD}/t_\mathrm{DPD}$, we can show that

$$\frac{m}{2}\left\langle\left(\frac{d_\mathrm{DPD}r_\mathrm{C}}{t_\mathrm{DPD}\tau_\mathrm{C}}\right)^2\right\rangle = \frac{3}{2}k_\mathrm{B}T \tag{A3}$$

$$\left(\frac{r_\mathrm{C}}{\tau_\mathrm{C}}\right)^2 m\left\langle\left(\frac{d_\mathrm{DPD}}{t_\mathrm{DPD}}\right)^2\right\rangle = 3k_\mathrm{B}T \tag{A4}$$

$$\left(\frac{r_\mathrm{C}}{\tau_\mathrm{C}}\right)^2 = \frac{k_\mathrm{B}T}{m}. \tag{A5}$$

Using $k_\mathrm{B}T = 4.11 \times 10^{-21}$ J at room temperature, and the previously calculated values of $r_\mathrm{C} = 5.65 \times 10^{-10}$ m and $m = 5.98 \times 10^{-26}$ kg, finds a value for the time scale of $\tau_\mathrm{C} = 2.16 \times 10^{-12}$ s.

Appendix B: Relationship between Γ and Schmidt number

We investigated how the Stoyanov-Groot thermostat behaves when applied to a simple simulation case. This allowed us to choose appropriate Γ values for our simulations. A variety of simulations were performed on simulation boxes containing only water beads with box size $L = 20$. We calculate the viscosity using Eq. 14 and use a shear rate of $\dot{\gamma} = 0.006$. The diffusion coefficient D is calculated using the mean squared displacement

$$D = \frac{\langle(\mathbf{r}(t) - \mathbf{r}_0)^2\rangle}{2td}, \tag{B1}$$

where $\mathbf{r}_0$ is the initial position at time $t = 0$, d is the number of dimensions of the simulation box (in this case $d = 3$), and the angled brackets indicate an average over all beads. We vary the collision frequency Γ and time step Δt. The Schmidt number can be calculated from the viscosity and diffusion coefficient.

Fig. 20 shows the relationship between Γ and the Schmidt number, confirming a $\mathrm{Sc} \propto \Gamma^2$ relationship. This relationship breaks down for high values of $\Gamma \Delta t$. Therefore, in order to increase the Schmidt number by increasing the collision parameter, may require a decrease in the time step.

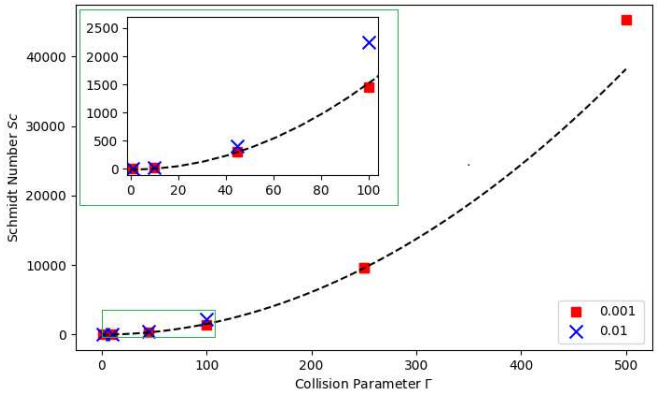

FIG. 20: Relationship between collision parameter Γ and resulting Schmidt number of bulk water. Two time steps $\Delta t = 0.01$ and $\Delta t = 0.001$ are tested. A fit of the form $\mathrm{Sc} = A\Gamma^2 + B$, where A and B are constants, is applied to the points from the $\Delta t = 0.001$ for $\Gamma \leq 250$.

Appendix C: Collision parameter Γ and the auto-correlation function

For simulation boxes consisting of pure water, the viscosity is calculated using a variety of different Γ choices, and a selection of autocorrelation functions are illustrated in Fig. 21. It is shown that as the value of Γ increases (*i.e.* the friction increases), the autocorrelation function decays more rapidly. This poses a problem for using this method (based upon integration over time) at high Γ values.

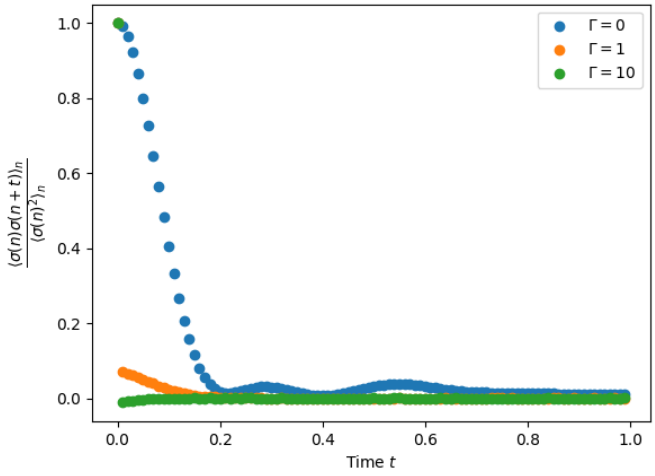

FIG. 21: Examples of the autocorrelation functions obtained for different values of the collision parameter Γ.

[1] R. L. Hendrikse, A. E. Bayly, and P. K. Jimack, "Studying the structure of sodium lauryl ether sulfate solutions using dissipative particle dynamics," The Journal of Physical Chemistry B **126**, 8058–8071 (2022).

[2] A. S. Poulos, C. S. Jones, and J. T. Cabral, "Dissolution of anionic surfactant mesophases," Soft matter **13**, 5332–5340 (2017).

[3] G. Montalvo and A. Khan, "Rheological properties of a surfactant-induced gel for the lysozyme–sodium dodecyl sulfate–water system," Colloid and Polymer Science **283**, 402–412 (2005).

[4] L. Kushner, B. Duncan, and J. Hoffman, "A viscometric study of the micelles of sodium dodecyl sulfate in dilute solutions," Journal of research of the National Bureau of Standards **49**, 85–90 (1952).

[5] M. Yiannourakou, B. Rousseau, N. Pannacci, and B. Herzhaft, "Rheological behavior of aqueous polyacrylamide solutions determined by dissipative particle dynamics and comparison to experiments," Europhysics Letters **97**, 34007 (2012).

[6] S. Bair, C. McCabe, and P. T. Cummings, "Comparison of nonequilibrium molecular dynamics with experimental measurements in the nonlinear shear-thinning regime," Physical Review Letters **88**, 058302 (2002).

[7] H. Droghetti, I. Pagonabarraga, P. Carbone, P. Asinari, and D. Marchisio, "Dissipative particle dynamics simulations of triblock co-polymer and water: Phase diagram validation and microstructure identification," The Journal of Chemical Physics **149**, 184903 (2018).

[8] C. Espinoza, M. Simmons, F. Alberini, O. Mihailova, D. Rothman, and A. Kowalski, "Flow studies in an in-line silverson 150/250 high shear mixer using PIV," Chemical Engineering Research and Design **132**, 989–1004 (2018).

[9] J. Eastoe, T. F. Towey, B. H. Robinson, J. Williams, and R. K. Heenan, "Structures of metal bis(2-ethylexyl) sulfosuccinate aggregates in cyclohexane," Journal of Physical Chemistry **97**, 1459–1463 (1993).

[10] K. ud Din, S. L. David, and S. Kumar, "Viscosities of sodium dodecyl sulfate solutions in aqueous ammonium salts," Journal of Chemical & Engineering Data **42**, 1224–1226 (1997).

[11] D. Calvo, J. L. Ruiz, and M. Valiente, "Phase equilibria of mixtures of surfactants and viscoelastic properties of the liquid crystal phases," Fluid Phase Equilibria **425**, 358–364 (2016).

[12] C. Gallegos, J. M. Franco, and F. Cordobés, "Rheology of the lamellar liquid-crystalline phase in polyethoxylated alcohol/water/heptane systems," Grasas y aceites (Sevilla) **56**, 96–105 (2005).

[13] M. R. Alcantara and L. C. F. Dias, "The cholesterization process on lyotropic liquid crystals studied by rheology," Colloids and Surfaces. A, Physicochemical and Engineering Aspects **136**, 155–158 (1998).

[14] G. Chauhan, K. Ojha, and A. Baruah, "Effects of nanoparticles and surfactant charge groups on the properties of VES gel," Brazilian Journal of Chemical Engineering **34**, 241–251 (2017).

[15] H. Li, L. Dang, S. Yang, J. Li, and H. Wei, "The study of phase behavior and rheological properties of lyotropic liquid crystals in the LAS/AES/H_2O system," Colloids and Surfaces. A, Physicochemical and Engineering Aspects **495**, 221–228 (2016).

[16] J. Zhaoa, Z. Wanga, X. Weib, F. Liuc, W. Zhoua, X. Tanga, and T. Wua, "Phase behaviour and rheological properties of the lamellar liquid crystals formed in dodecyl polyoxyethylene polyoxypropylene ether/water system," Indian Journal of Chemistry - Section A Inorganic, Physical, Theoretical and Analytical Chemistry **50**, 641–649 (2011).

[17] S. Meng, J. Zhang, Y. Wang, X. Li, C. Wu, T. Hou, L. Xiao, and G. Lu, "Simulating the rheology of surfactant solution using dissipative particle dynamics," Molecular Simulation **41**, 772–778 (2015).

[18]E. Boek, P. Coveney, H. Lekkerkerker, and P. v. d. Schoot, "Simulating the rheology of dense colloidal suspensions using dissipative particle dynamics," Physical Review. E **55**, 3124–3133 (1997).
[19]B. L. Peters, A. Ramírez-Hernández, D. Q. Pike, M. Müller, and J. J. de Pablo, "Nonequilibrium simulations of lamellae forming block copolymers under steady shear: A comparison of dissipative particle dynamics and brownian dynamics," Macromolecules **45**, 8109–8116 (2012).
[20]H. Zhang, D. Li, L. Pei, L. Zhang, and F. Wang, "The stability of the micelle formed by chain branch surfactants and polymer under salt and shear force: Insight from dissipative particle dynamics simulation," Journal of Dispersion Science and Technology **37**, 270–279 (2016).
[21]P. Xu, J. Lin, L. Wang, and L. Zhang, "Shear flow behaviors of rod-coil diblock copolymers in solution: A nonequilibrium dissipative particle dynamics simulation," The Journal of Chemical Physics **146**, 184903 (2017).
[22]C. M. Wijmans and B. Smit, "Simulating tethered polymer layers in shear flow with the dissipative particle dynamics technique," Macromolecules **35**, 7138–7148 (2002).
[23]Y. Shan, X. Qiang, J. Ye, X. Wang, L. He, and S. Li, "Shear-induced microstructures and dynamics processes of phospholipid cylinders in solutions," Scientific Reports **9**, 15393–15 (2019).
[24]R. D. Groot and P. B. Warren, "Dissipative particle dynamics: Bridging the gap between atomistic and mesoscopic simulation," The Journal of Chemical Physics **107**, 4423–4435 (1997).
[25]V. Symeonidis, G. E. Karniadakis, and B. Caswell, "Schmidt number effects in dissipative particle dynamics simulation of polymers," The Journal of Chemical Physics **125**, 184902 (2006).
[26]T. F. Clarke, *Rheological characterization of polymers via dissipative particle dynamics*, Ph.D. thesis, Massachusetts Institute of Technology. Dept. of Chemical Engineering. (2008).
[27]W. Richtering, J. Laeuger, and R. Linemann, "Shear orientation of a micellar hexagonal liquid crystalline phase: A rheological and small angle light scattering study," Langmuir **10**, 4374–4379 (1994).
[28]T. Tepe, M. Schulz, J. Zhao, M. Tirrell, F. Bates, K. Mortensen, and K. Almadal, "Variable shear-induced orientation of a diblock copolymer hexagonal phase," Macromolecules **28**, 3008–3011 (1995).
[29]C. E. Fairhurst, M. C. Holmes, and M. S. Leaver, "Shear alignment of a rhombohedral mesh phase in aqueous mixtures of a long chain nonionic surfactant," Langmuir **12**, 6336–6340 (1996).
[30]G. Schmidt, S. Müller, P. Lindner, C. Schmidt, and W. Richtering, "Shear orientation of lyotropic hexagonal phases," The Journal of Physical Chemistry. B **102**, 507–513 (1998).
[31]J. Berghausen, J. Zipfel, O. Diat, T. Narayanan, and W. Richtering, "Lamellar phases under shear: variation of the layer orientation across the couette gap," Physical Chemistry Chemical Physics **2**, 3623–3626 (2000).
[32]J. Zipfel, J. Berghausen, G. Schmidt, P. Linder, P. Alexandridis, M. Tsianou, and W. Richtering, "Shear induced structures in lamellar phases of amphiphilic block copolymers," Physical Chemistry Chemical Physics **1**, 3905–3910 (1999).
[33]F. N. Olivier Diat, Didier Roux, "Effect of shear on a lyotropic lamellar phase," Journal de Physique II **3**, 1427–1452 (1993).
[34]H. Guo, "Shear-induced parallel-to-perpendicular orientation transition in the amphiphilic lamellar phase: A nonequilibrium molecular-dynamics simulation study," The Journal of Chemical Physics **124**, 054902 (2006).
[35]K. Koppi, M. Tirrell, F. Bates, K. Almdal, and R. Colby, "Lamellae orientation in dynamically sheared diblock copolymer melts," Journal of Physics B Atomic and Molecular Physics **2**, 1941–1959 (1992).
[36]R. L. Anderson, D. J. Bray, A. Del Regno, M. A. Seaton, A. S. Ferrante, and P. B. Warren, "Micelle formation in alkyl sulfate surfactants using dissipative particle dynamics," Journal of Chemical Theory and Computation **14**, 2633–2643 (2018).
[37]P. Español and P. Warren, "Statistical mechanics of dissipative particle dynamics," Europhysics Letters **30**, 191–196 (1995).
[38]C. Marsh, G. Backx, and M. Ernst, "Static and dynamic properties of dissipative particle dynamics," Physical Review. E **56**, 1676–1691 (1997).
[39]S. D. Stoyanov and R. D. Groot, "From molecular dynamics to hydrodynamics: a novel galilean invariant thermostat," The Journal of Chemical Physics **122**, 114112 (2005).
[40]C. P. Lowe, "An alternative approach to dissipative particle dynamics," Europhysics Letters **47**, 145–151 (1999).
[41]D. J. Evans and B. L. Holian, "The Nose–Hoover thermostat," The Journal of Chemical Physics **83**, 4069–4074 (1985).
[42]E. Helfand, "Transport coefficients from dissipation in a canonical ensemble," Physical Review **119**, 1–9 (1960).
[43]B. Hess, "Determining the shear viscosity of model liquids from molecular dynamics simulations," The Journal of Chemical Physics **116**, 209–217 (2002).
[44]A. W. Lees and S. F. Edwards, "The computer study of transport processes under extreme conditions," Journal of Physics C: Solid State Physics **5**, 1921–1928 (1972).
[45]A. Chatterjee, "Modification to lees–edwards periodic boundary condition for dissipative particle dynamics simulation with high dissipation rates," Molecular Simulation **33**, 1233–1236 (2007).
[46]A. Moshfegh and A. Jabbarzadeh, "Modified lees–edwards boundary condition for dissipative particle dynamics: hydrodynamics and temperature at high shear rates," Molecular Simulation **41**, 1264–1277 (2015).
[47]J. H. Irving and K. J. G, "The statistical mechanical theory of transport processes. IV. the equations of hydrodynamics," The Journal of Chemical Physics **18** (1950).
[48]I. Stewart, *The Static and Dynamic Continuum Theory of Liquid Crystals: A Mathematical Introduction*, Liquid Crystals Book Series (CRC Press, 2019).
[49]M. Jonstroemer, B. Joensson, and B. Lindman, "Self-diffusion in nonionic surfactant-water systems," The Journal of Physical Chemistry **95**, 3293–3300 (1991).
[50]M. Holz, S. R. Heil, and A. Sacco, "Temperature-dependent self-diffusion coefficients of water and six selected molecular liquids for calibration in accurate 1H NMR PFG measurements," Physical Chemistry Chemical Physics **2**, 4740–4742 (2000).
[51]A. S. Poulos, D. Constantin, P. Davidson, M. Impéror, P. Judeinstein, and B. Pansu, "A PGSE-NMR study of molecular self-diffusion in lamellar phases doped with polyoxometalates," The Journal of Physical Chemistry B **114**, 220–227 (2010).
[52]G. Chidichimo, D. De Fazio, G. Ranieri, and M. Terenzi, "Self-diffusion of water in a lamellar lyotropic liquid crystal: A study by pulsed field gradient NMR," Chemical Physics Letters **117**, 514–517 (1985).
[53]B. Hammouda, "Temperature effect on the nanostructure of SDS micelles in water," Journal of Research of the National Institute of Standards and Technology **118**, 151–167 (2013).
[54]M. Ludwig, R. Geisler, S. Prévost, and R. von Klitzing, "Shape and structure formation of mixed nonionic-anionic surfactant micelles," Molecules (Basel, Switzerland) **26**, 4136– (2021).
[55]S. Khodaparast, W. N. Sharratt, G. Tyagi, R. M. Dalgliesh, E. S. Robles, and J. T. Cabral, "Pure and mixed aqueous micellar solutions of sodium dodecyl sulfate (SDS) and dimethyldodecyl amine oxide (DDAO): Role of temperature and composition," Journal of Colloid and Interface Science **582**, 1116–1127 (2021).
[56]X. Guo, X. Chen, W. Zhou, and J. Wei, "Effect of polymer drag reducer on rheological properties of rocket kerosene solutions," Materials **15** (2022), 10.3390/ma15093343.
[57]S. Wang, "Shear induced deformation of polymers: Calculation of radii of gyration," The Journal of Chemical Physics **92**, 7618–7624 (1990).
[58]P. Lindner and R. Oberthür, "Shear induced deformation of polystyrene in dilute solution from sans," Physica B: Condensed Matter **156-157**, 410–413 (1989).
[59]R. L. Hendrikse, A. E. Bayly, P. K. Jimack, and X. Lai, "Using raman spectroscopy and molecular dynamics to study conforma-

tion changes of sodium lauryl ether sulfate molecules (in press)," The Journal of Physical Chemistry B (2023).
[60]L.-Y. You, L.-J. Chen, H.-J. Qian, and Z.-Y. Lu, "Microphase transitions of perforated lamellae of cyclic diblock copolymers under steady shear," Macromolecules **40**, 5222–5227 (2007).
[61]M. Lísal and J. K. Brennan, "Alignment of lamellar diblock copolymer phases under shear: Insight from dissipative particle dynamics simulations," Langmuir **23**, 4809–4818 (2007).
[62]A. Chremos, P. M. Chaikin, R. A. Register, and A. Z. Panagiotopoulos, "Shear-induced alignment of lamellae in thin films of diblock copolymers," Soft Matter **8**, 7803–7811 (2012).
[63]R. Larson, *The Structure and Rheology of Complex Fluids*, Topics in Chemical Engineering (OUP USA, 1999).
[64]F. Nettesheim, I. Grillo, P. Lindner, and W. Richtering, "Shear-induced morphology transition and microphase separation in a lamellar phase doped with clay particles," Langmuir **20**, 3947–3953 (2004).
[65]T. Kato, K. Minewaki, Y. Kawabata, M. Imai, and Y. Takahashi, "Anomalous decrease in lamellar spacing by shear flow in a nonionic surfactant/water system," Langmuir **20**, 3504–3508 (2004).
[66]S. J. Gray, M. Walker, R. Hendrikse, and M. R. Wilson, "Investigating anionic surfactant phase diagrams using dissipative particle dynamics: development of a transferable model," Soft Matter **19**, 3092–3103 (2023).